Electronic Supplementary Material (ESI) for RSC Advances.

ELECTRONIC SUPPLEMENTARY INFORMATION

Convenient Architectures of Cu_2O/SnO_2 Type II *p-n* Heterojunctions and their Application in Visible Light Catalytic Degradation of Rhodamine B

Shravanti Joshi, [a, b, d] *Samuel J. Ippolito,* [a, b, c] *and Sunkara V. Manorama* [b, d*]

[a] Centre for Advanced Materials and Industrial Chemistry (CAMIC), School of Science, College of Science, Engineering & Health, RMIT University, Melbourne, VIC 3001, Australia.

[b] RMIT-IICT Research Centre, CSIR-Indian Institute of Chemical Technology, Hyderabad - 500 007, India.

[c] School of Engineering, RMIT University, Melbourne, VIC 3001, Australia.

[d] Nanomaterials Laboratory, Inorganic & Physical Chemistry Division, CSIR-Indian Institute of Chemical Technology, Hyderabad - 500 007, India. E-mail address: manorama@iict.res.in, Tel.: +91 40 27193225; Fax: +91 40 27160921.

* *To whom all Correspondence should be addressed.*

Additional Characterization Techniques

The thermal stabilities of the nanocomposites were assessed by a TA Q50 thermo-gravimetric analyzer. Thermogravimetric scans were recorded at a ramp rate of 10oC/min under nitrogen atmosphere for 10 to 20 mg samples in the temperature range 35 to 800 oC. Analysis of the thermogram was carried out using universal analysis software provided by the TA instruments. Fourier transform infrared spectroscopy (FT-IR) was used to follow the formation of the nanocomposites in the mid-FTIR absorption range of 4000-400 cm-1 employing a Bruker ALPHA-T instrument. Typically, nanocomposite samples (~ 1 mg) were ground with KBr (~ 100 mg) and pressed into transparent pellets of approximate dimensions, D = 1.2 cm and t = 0.02 cm; followed by vacuum drying at 60oC for 30 minutes prior to each run. The transmittance spectra collected for 256 scans with a resolution interval 2 cm-1, were corrected for baseline, atmospheric interference and also normalized before comparative evaluation. The confocal micro-Raman spectroscopy was performed using a Horiba Jobin-Yvon LabRam HR spectrometer with a 17 mW internal He–Ne (Helium–Neon) laser source with excitation wavelength of 632.8 nm. Photoluminescence measurements were carried out using a HORIBA Jobin Yvon spectrofluorometer. Degree of mineralization of Rhodamine B was monitored by the total organic carbon (TOC) analysis of the aliquots drawn at different irradiation times using a TOC-L-CPH Shimadzu analyzer according to procedure supplied by Shimadzu company.

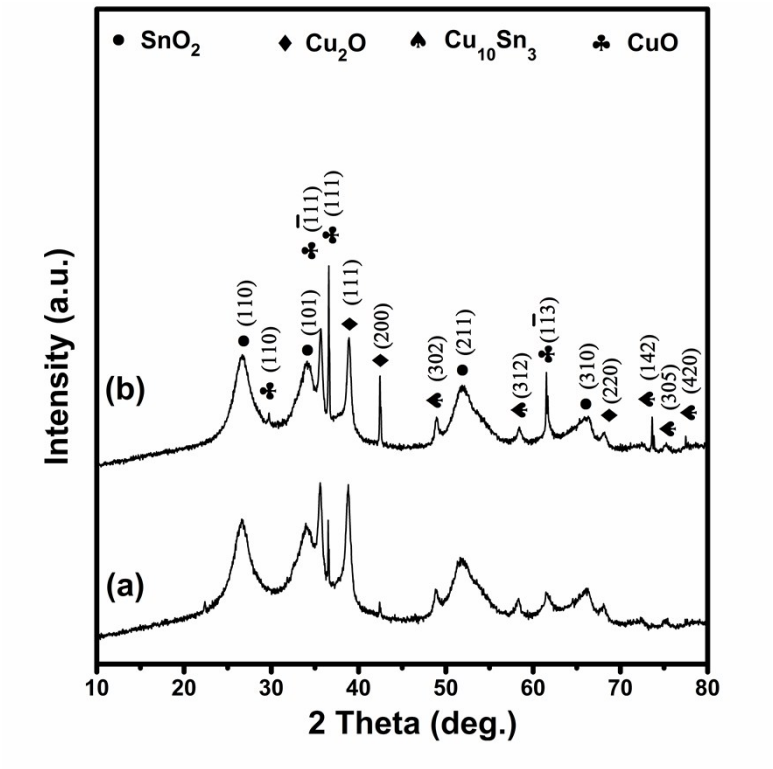

Fig. S1 Powder X-ray diffraction of Cu_2O/SnO_2 heterostructures obtained at 180 ^oC for 3 h via hydrothermal route, (a) in 1.5:1 and (b) in 2:1 mole ratio. [**SnO_2** - Space group: $P4_2/mmm$, JCPDS card no. 21-1250, **CuO** - Space group: C2/c (15), JCPDS card no. 80-0076, **Cu_2O** - Space group: $Pn\bar{3}m$ (224), JCPDS card no.77-0199 and **$Cu_{10}Sn_3$** - Space group: $P6_3$ (173), JCPDS card no. 65-2064].

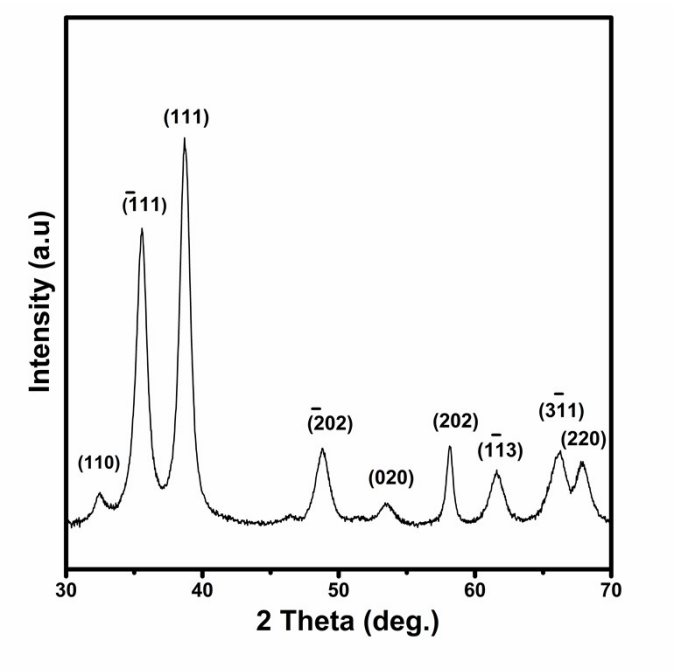

Fig. S2.1 Powder X-ray diffraction of mixed phase copper oxide obtained at 180 ^{o}C for 3 h via hydrothermal route (**Space group: C2/c (15), JCPDS card no. 80-0076**).

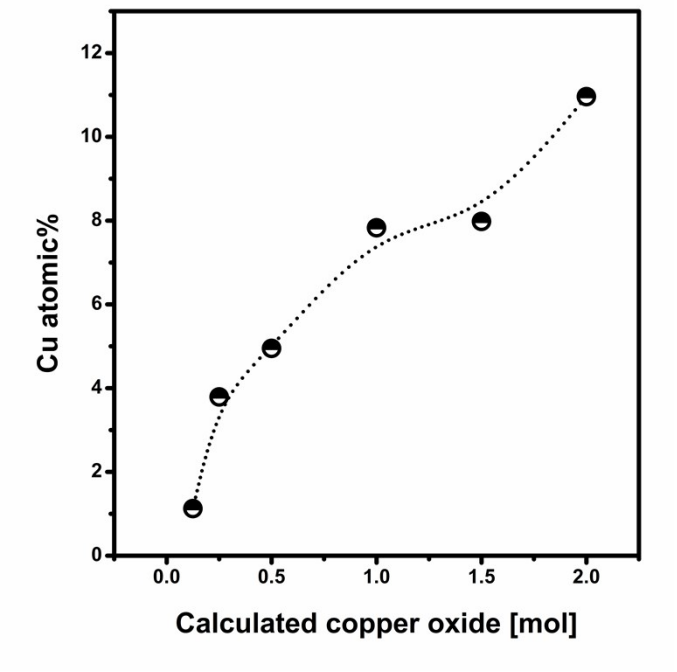

Fig. S2.2 Plot of copper loading amount as a function of theoretically calculated copper oxide concentration in moles.

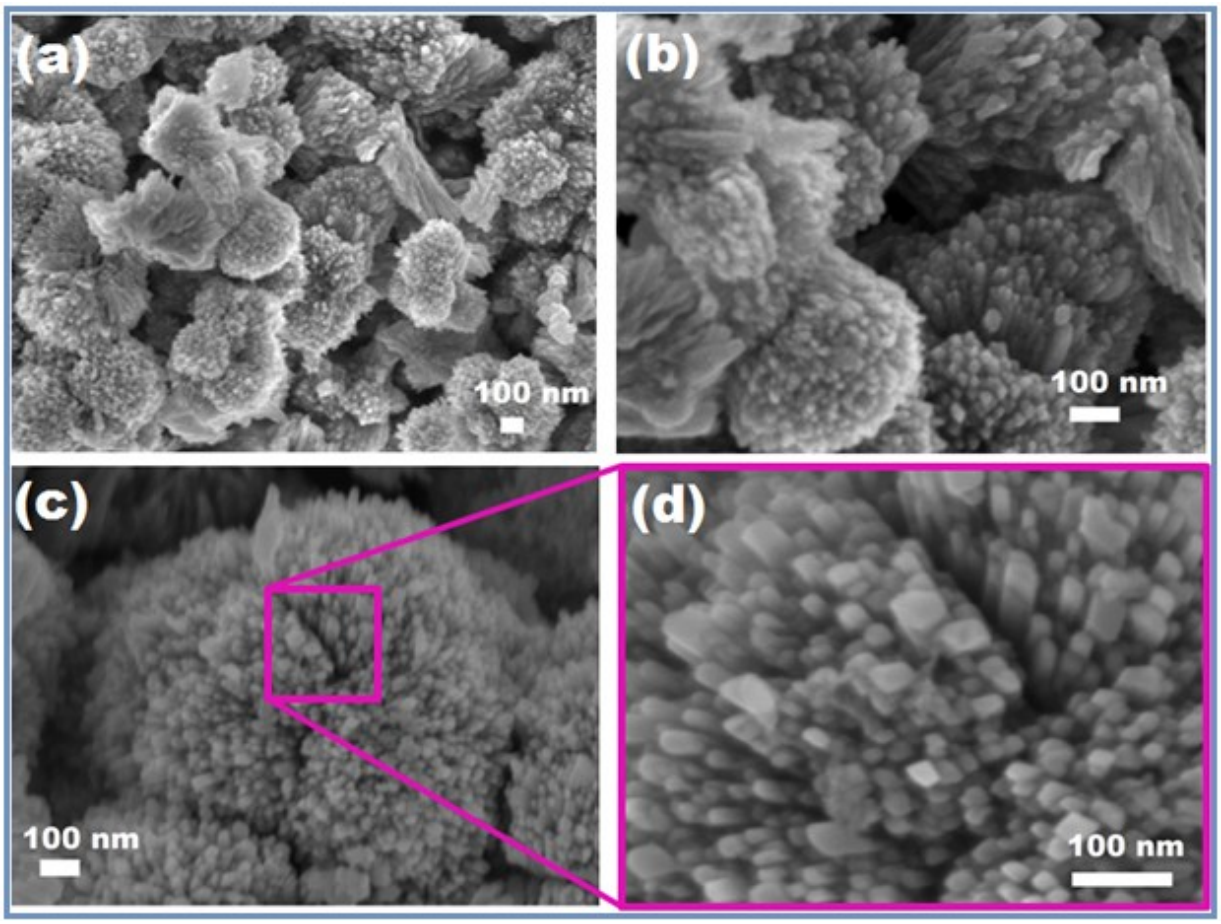

Fig. S2.3 (a-d) Series of micrographs depicting hierarchical structure of as synthesized mixed phase copper oxide.

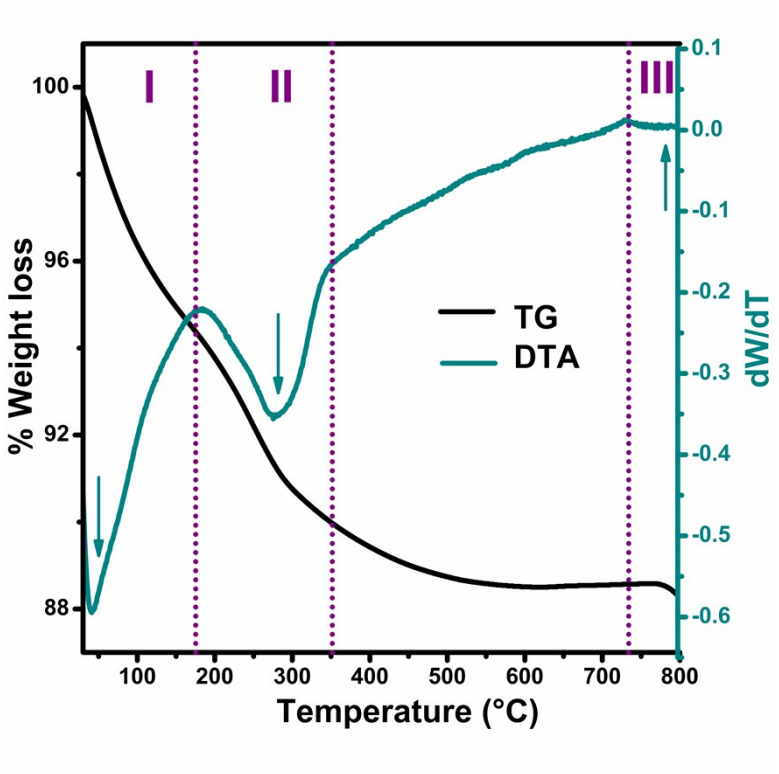

Fig. S3 TG-DTA trace under nitrogen atmosphere of 1:1 mole ratio Cu_2O/SnO_2 nanocomposite synthesized via hydrothermal route at 180 ^oC for 3 h.

Fig. **S3** clearly shows a three-step decomposition of nanocomposite. The first strong peak in the 35-150 ^oC region with weight loss of 5.06 % has been attributed to removal of surface adsorbed water and corresponds to endothermic peak at a temperature 43.38 ^oC in DTA spectra. The second weight loss in the range 168-350 ^oC is due to thermal decomposition of $CuAc_2.H_2O$. During this process there is a weight loss of 4.03 %. This thermal decomposition in air can be summarized in three main steps which are well documented in literature.[1] $CuAc_2.H_2O$ dehydrates around 168 ^oC; $CuAc_2$ decomposes to initial solid and volatile products at 168-302 ^oC; the initial solid products Cu and Cu_2O are oxidized to CuO in air at 302-500 ^oC. The copper acetate peroxides are found to form in the range 35-150 ^oC, and the dehydration of these peroxides results in the presence of $CuAc_2.H_2O$ above 168 ^oC. In the range 200-500 ^oC, weight loss of 5.04 % was observed which can be attributed to the desorption of O^- and O^{2-} during the dehydration process corresponding to the conversion of tin hydroxide to tin oxide as

well as progressive crystallization, and also charring of residual glucose agreeing well with our earlier reports.[2] The above sequence could be assumed to be valid during the hydrothermal synthesis also but at much lower temperatures.

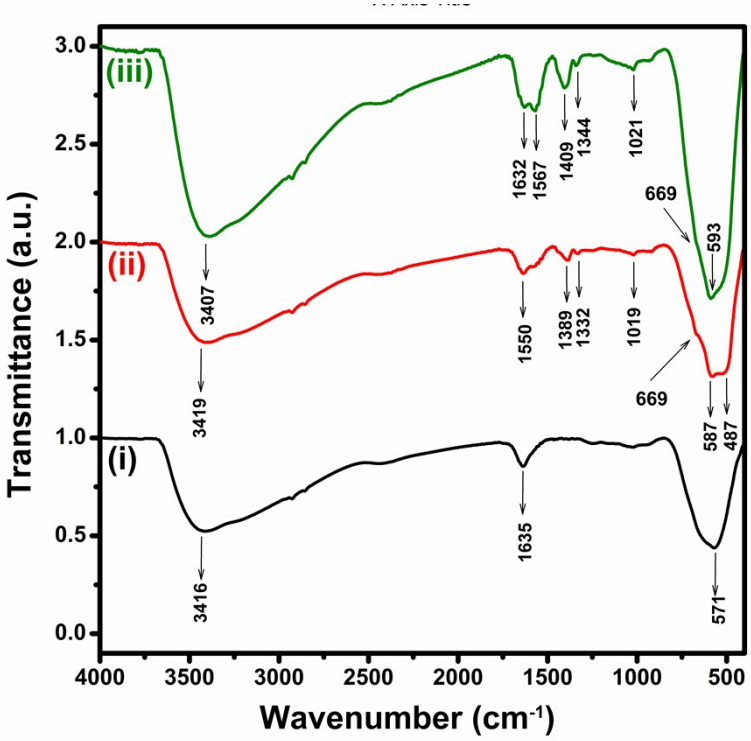

Fig. S4.a *mid*-FTIR spectra of as-synthesized **(i)** Pure SnO_2 nanospheres, **(ii)** Mixed phase copper oxide and **(iii)** Cu_2O/SnO_2 nanocomposite in 1:1 mole ratio, respectively depicting characteristic bands.

Fig. **S4.a** represents the FT-IR spectrum recorded for as synthesized photocatalysts. Fig. **S4 (i)** showcases pure SnO_2 spectrum that is in agreement with our earlier reports.[2] Fig. **S4.a (ii)**, the strong peak at 3419 cm^{-1} is assigned to the stretching vibration of the O–H bond, υ(OH), which indicates the presence of hydroxyl ions due to the metal-OH layer. The characteristic bands observed at 487 cm^{-1} and 587 cm^{-1} are due to monoclinic phase, can be assigned to the Au mode and Bu mode of CuO. The high-frequency mode at 487 cm^{-1} can be assigned to the

Cu-O stretching vibration along the [101] direction. A weak peak at 1019 cm^{-1} is ascribed to δ (OH).[3-7] The broad absorption bands between 1300 and 2000 cm^{-1} are mainly ascribed to the chemisorbed and/or physisorbed H_2O and CO_2 molecules on the surface of nanostructured hierarchical crystals of copper oxide. Also the presence of broad absorption peak in the range 605 - 670 cm^{-1} corresponding to the infrared active mode of Cu_2O confirms that the synthesized product is mixed phase of copper oxide, [8-10] in good agreement with X-ray diffractograms (See Fig. **S1** and Fig. **S2.1**). Fig. **S4.a (iii)** confirms nanocomposite formation as bands pertaining to both Cu_2O and SnO_2 are present hence validating the presence of only these materials in the nanocomposite.

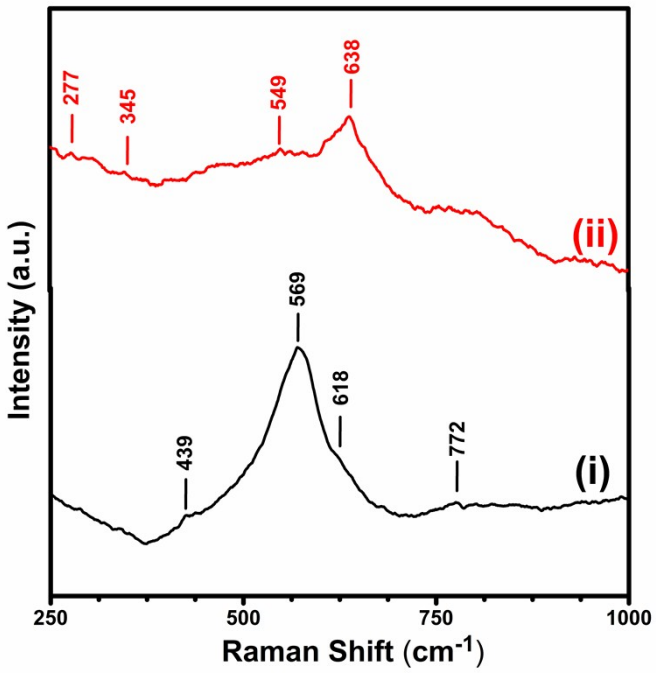

Fig. S4.b Stacked micro-Raman spectra using 632.8 nm laser of **(i)** Pure SnO_2 nanospheres and **(ii)** Cu_2O/SnO_2 heterostructures in 1:1 mole ratio obtained at 180 ^oC for 3 h via hydrothermal route depicting characteristic modes.

Fig. **S4.b (i)** shows the room-temperature Raman spectrum of pure SnO_2 nanospheres belonging to the space group D_{4h}^{14}. Three fundamental peaks observed at 439, 618 and 772 cm^{-1} corresponds to the E_g and two normal phonon modes A_{1g} and B_{2g} related to the expansion and contraction vibration mode of Sn-O bonds commonly found in bulk single or polycrystalline SnO_2 respectively[12,13]. These peak positions further confirm the structure in tetragonal rutile form. Furthermore to these classical vibration modes, Raman scattering peak at 569 cm^{-1} can be assigned to surface defects of SnO_2, and is attributed to the surface phonon mode. This phenomenon is assumed to be related to microstructure of SnO_2 nanospheres where particle size is observed to be in nanoscale region[14,15]. Similar peak shifts have been reported in case of SnO/SnO_2 nanocomposites[15], SnO_2 nanorods[16] and nanoparticles[17]. Trace **(ii)** in the Fig. **S4.b** shows Raman spectrum of Cu_2O/SnO_2 heterostructures in 1:1 mole ratio. The major portion of peak at 638 cm^{-1} can be readily attributed to infrared allowed mode of Cu_2O[18-21], while the low intensity Raman peaks at 277 and 345 cm^{-1} belong to CuO phase and are consistent with spectra reported in literature[22-24]. Cu_2O/SnO_2 nanocomposite in addition to SnO_2 here is composed of both CuO and Cu_2O nanoparticles hence we believe that surface as well as interface atoms will be in disordered sates. Therefore some of the vibrational modes show reduced Raman intensity for e.g. visibly blue shifted peak at 549 cm^{-1} pertaining to impregnation of copper oxides in SnO_2 in equal mole ratio[24].

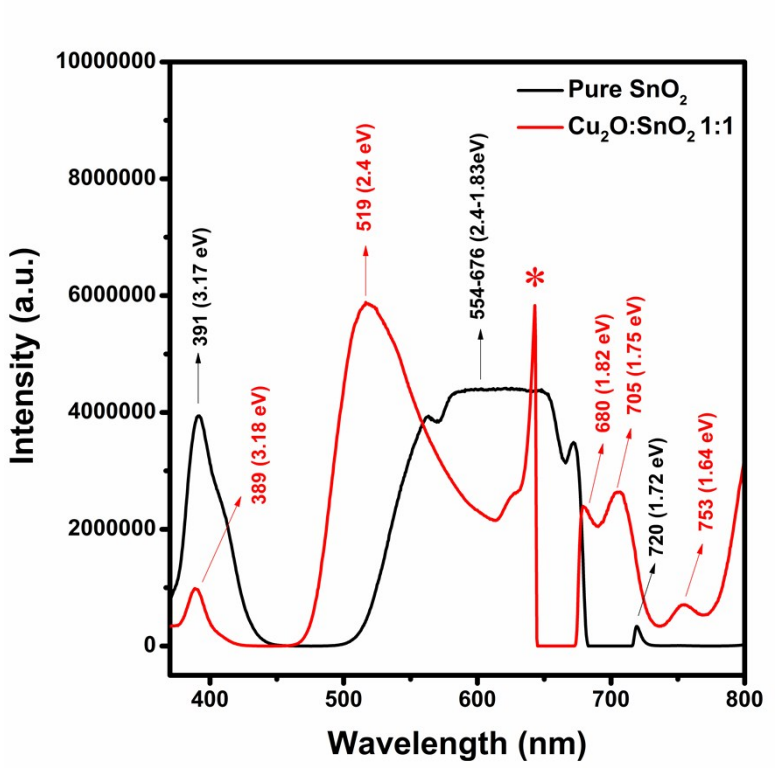

Fig. S4.c Photoluminescence spectrum of pure SnO_2 and Cu_2O/SnO_2 nanocomposite in 1:1 mole ratio excited at 350 nm (* represents peak due to Xenon lamp).

Peak positions observed from PL spectrum gives information about interface and impurity levels, identification of surface defects and a correlation of fluorescence/phosphorescence activities[25]. But in environmental remediation application such as semiconductor mediated photocatalysis, photoluminescence spectrum is used to derive greater insights associated with relative rates of charge carrier trapping, its migration and transfer[26]. It has been widely reported, that a decrease in PL intensity indicates a decrease in the recombination rate and thus an enhanced charge separation efficiency of photoinduced electrons and holes. A comparative room temperature photoluminescence spectrum of pure SnO_2 and Cu_2O/SnO_2 nanocomposite in 1:1 mole ratio is shown in Fig. **S4.c** with the excitation wavelength at 350 nm. Trace of pure SnO_2 depicts a peak position at 391 nm (3.17 eV) which can be attributed to the characteristic

band-band PL phenomenon associated with photogenerated charge carriers and is consistent with earlier reports observed in case of SnO_2 nanostructures[27].The strong luminescence band in the range 554-676 nm might be related to crystal defects and residual stresses that have appeared during the growth[28]. One weak emission band centered at 720 nm (1.72 eV) belongs to red emission band. In accordance with earlier hypothesis yellow, orange and red emissions are attributed to oxygen vacancies and luminescent centres formed by tin interstitials thus indicating presence of several sub states related to the involving defect centres. Additionally, the blue-green and yellow emission regions are due to singly and doubly charged oxygen vacancies in depletion region of *n*-type semiconductor metal oxide[29-32].

PL trace of Cu_2O/SnO_2 nanocomposite in 1:1 mole ratio shows characteristic bands of SnO_2 as well as copper oxides. Luminescence band at 389 nm (3.18 eV) showed decreased intensity and as mentioned above belongs to SnO_2. The emissions at 519 nm (2.4 eV) and 753 nm (1.64 eV) matches the bandgap of Cu_2O and CuO nanostructures respectively and are thereby attributed to near band-edge transitions from free or bound exciton recombination[33]. Band-band transition of SnO_2 reduced drastically in intensity for the nanocomposite owing to impairment in recombination of electron-hole pair in Cu_2O/SnO_2 heterostructure, thereby favouring photocatalysis reaction.

Spectrum processing :

No peaks omitted

Processing option : All elements analyzed (Normalised)

Number of iterations = 3

Standard :

C CaCO3 1-Jun-1999 12:00 AM

O SiO2 1-Jun-1999 12:00 AM

Cu Cu 1-Jun-1999 12:00 AM

Sn Sn 1-Jun-1999 12:00 AM

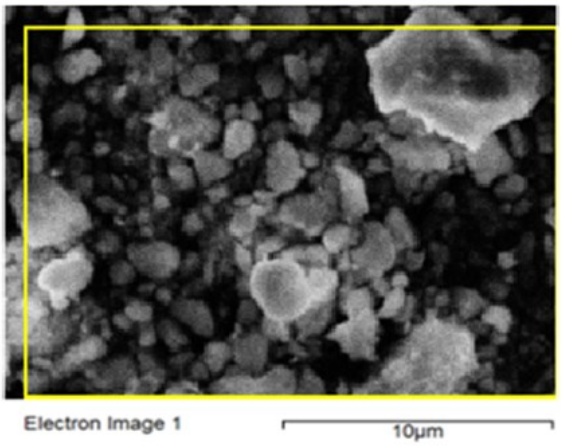

Element	Weight%	Atomic%
C K	6.00	15.59
O K	33.98	66.32
Cu L	10.08	4.95
Sn L	49.95	13.14
Totals	100.00	

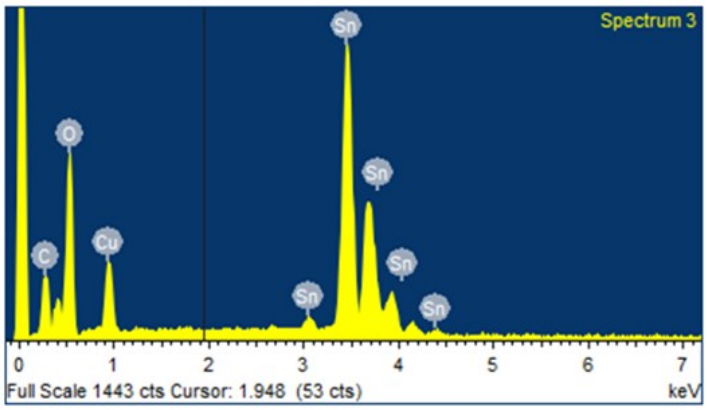

Fig. S5 Elemental quantification of 0.5:1 mole ratio Cu_2O/SnO_2 nanocomposite before visible light induced Rhodamine B photodegradation.

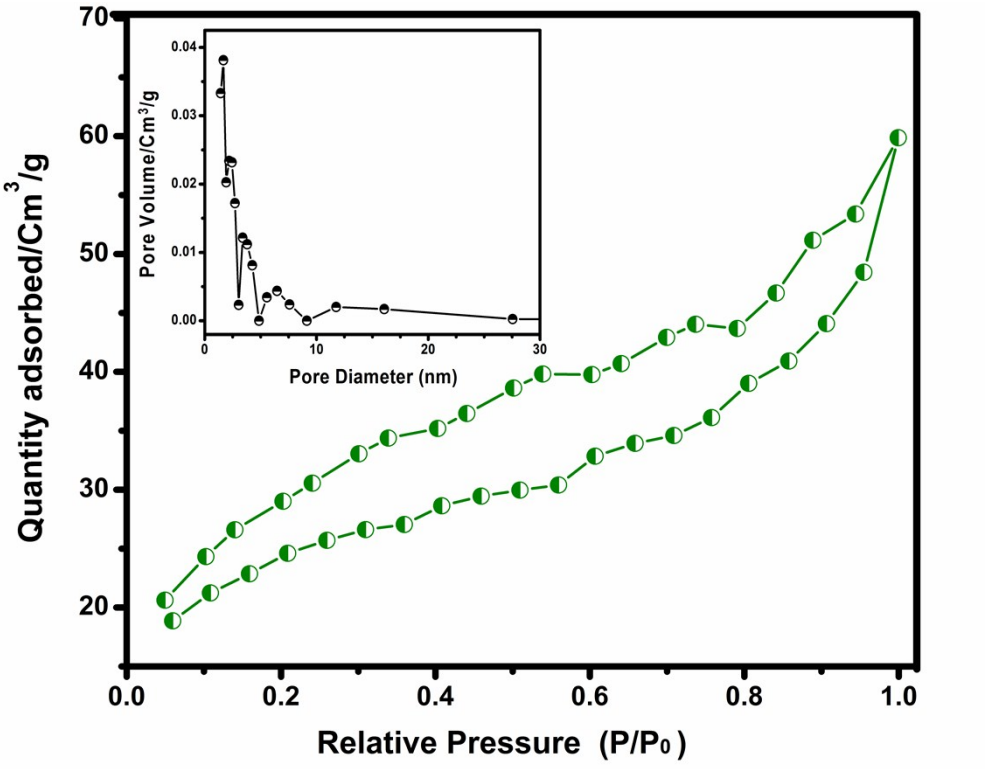

Fig. S6 N_2 adsorption–desorption BJH isotherms of 1:1 mole ratio Cu_2O/SnO_2 nanocomposite.

Inset: Corresponding Barret-Joyner-Halenda (BJH) pore size distributions.

P/P_0	Volume [cc/g] STP	$1/(W((P_0/P)-1))$
5.9680E-02	18.8584	2.693E+00
1.0858E-01	21.2339	4.590E+00
1.5908E-01	22.8537	6.623E+00
2.0867E-01	24.5980	8.578E+00
2.5934E-01	25.6990	1.090E+01
3.0941E-01	26.6083	1.347E+01

BET Summary

Surface Area = 81.61 m²/g

Slope = 42.73, Y - Intercept = 5.830E-02

Correlation Coefficient, r = 0.99848, C constant= 732.0

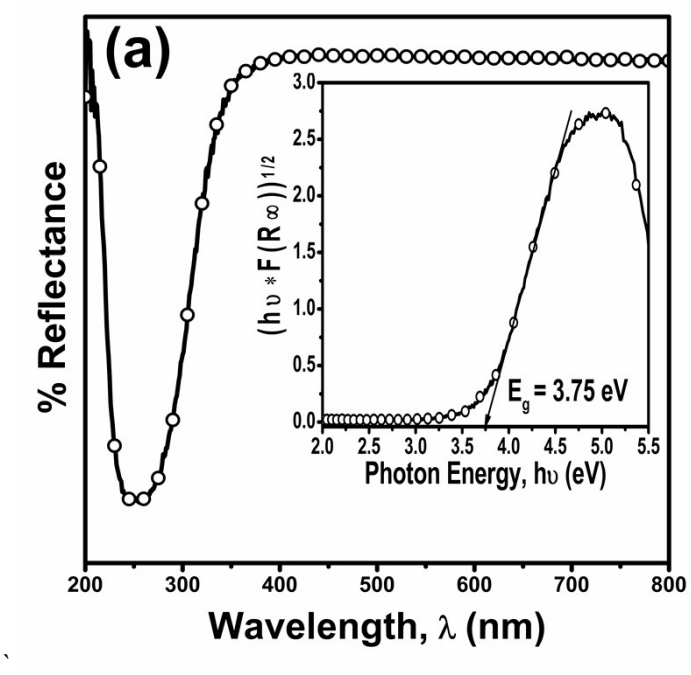

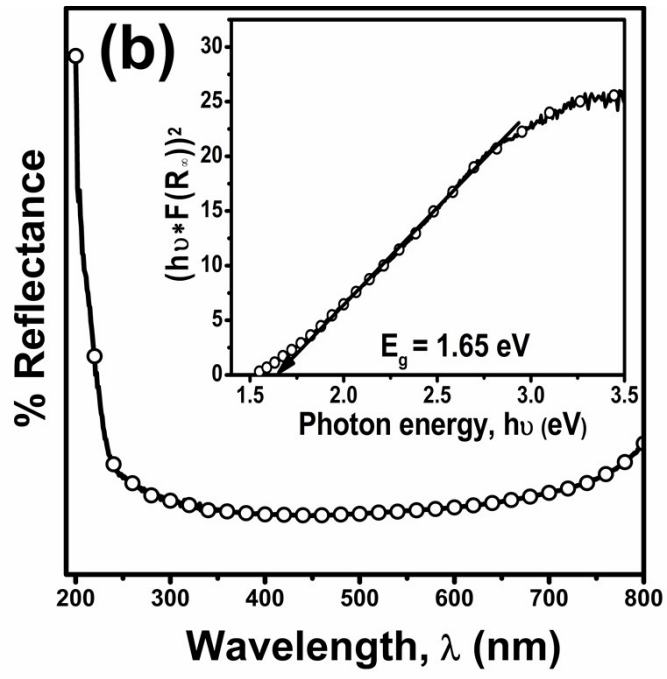

Fig. S7 UV-vis diffused reflectance spectra of as-synthesized, **(a)** Pure SnO_2 and **(b)** Mixed phase copper oxide. **Inset:** Schuster-Kubelka-Munk remission functions, [hυ.F (R_∞)] plotted as a function of energy (E_g) to estimate optical bandgap.

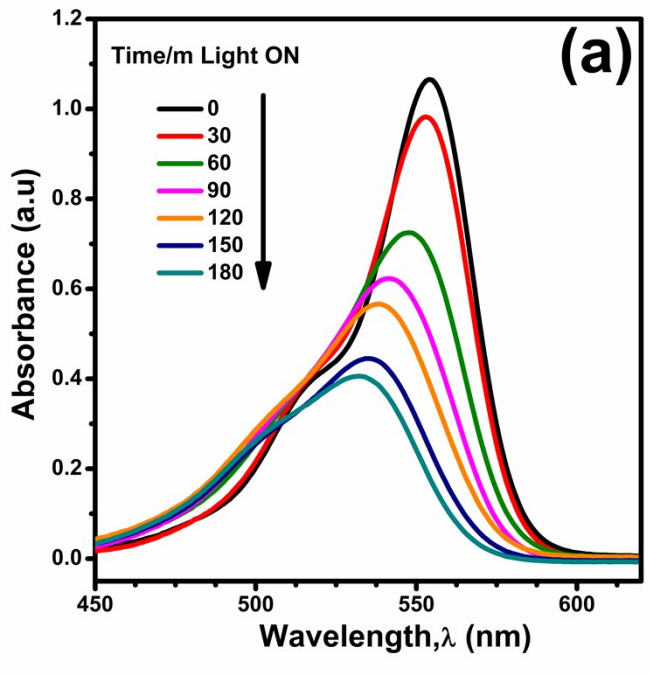

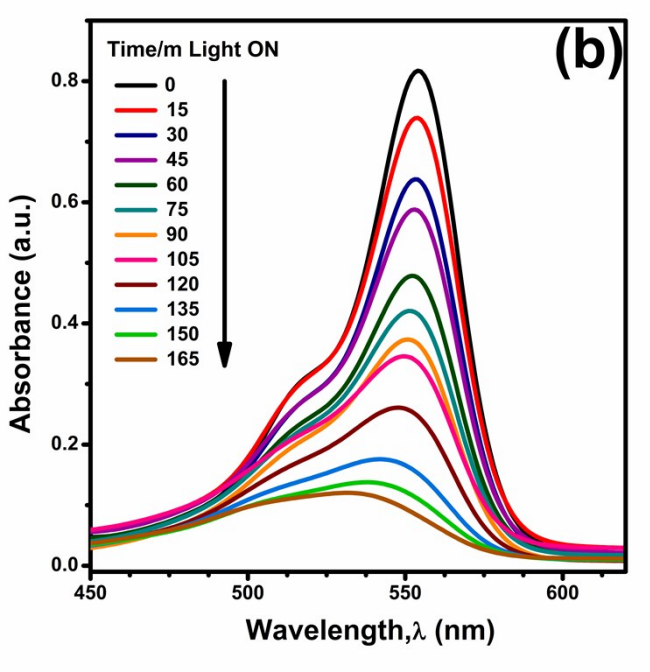

Fig. S8 Absorbance spectra depicting the change in concentration of RhB under visible irradiation as a function of time namely **(a)** Pure SnO_2 and **(b)** Mixed phase copper oxide.

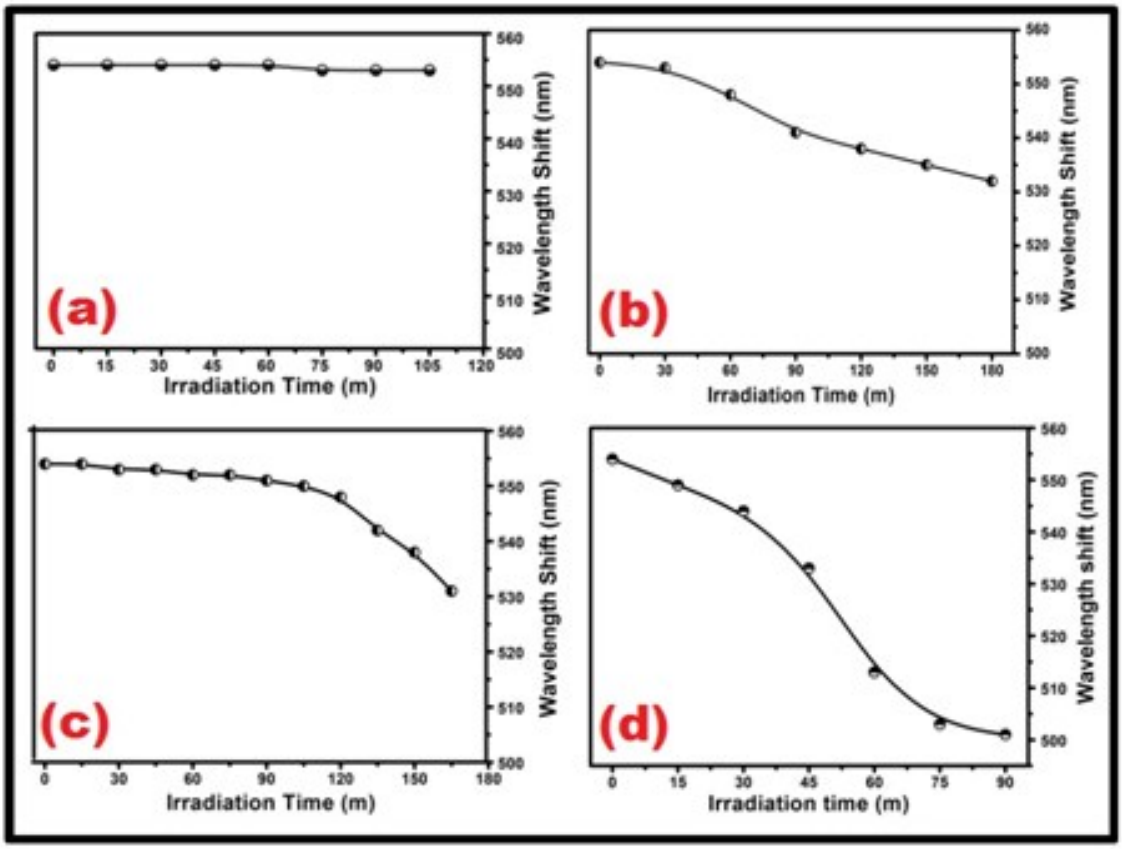

Fig. S9 Absorption maximum shift as function of irradiation time in minutes, where **(a)** Degradation profile of RhB in absence of nanocomposite, **(b)** Pure SnO_2 nanospheres, **(c)** Mixed phase copper oxide and **(d)** 1:1 mole ratio Cu_2O/SnO_2 nanocomposite.

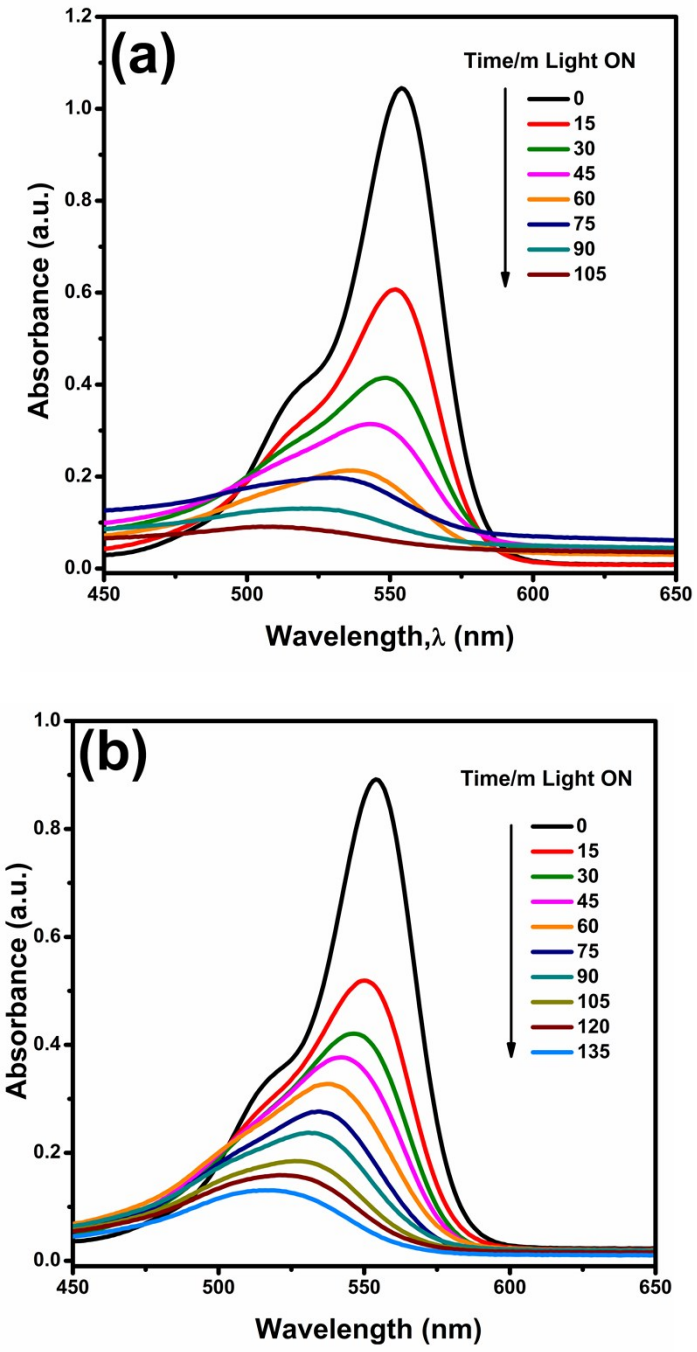

Fig. S10 Absorbance spectra depicting the change in concentration of RhB over nanocomposite under visible irradiation as a function of time namely, **(a)** Cu_2O/SnO_2 = 0.5:1, and **(b)** Cu_2O/SnO_2 = 0.25:1.

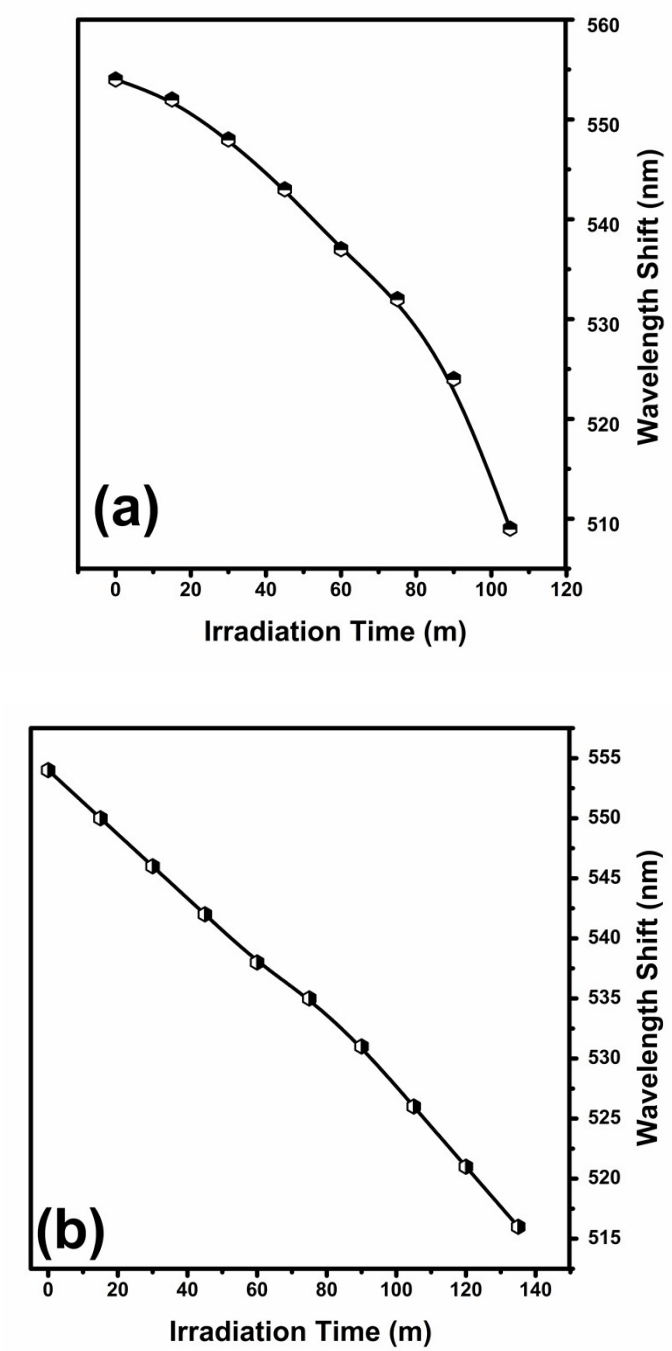

Fig. S11 Absorption maximum shift as a function of irradiation time in minutes, **(a)** Cu_2O/SnO_2 = 0.5:1 and **(b)** Cu_2O/SnO_2 = 0.25:1.

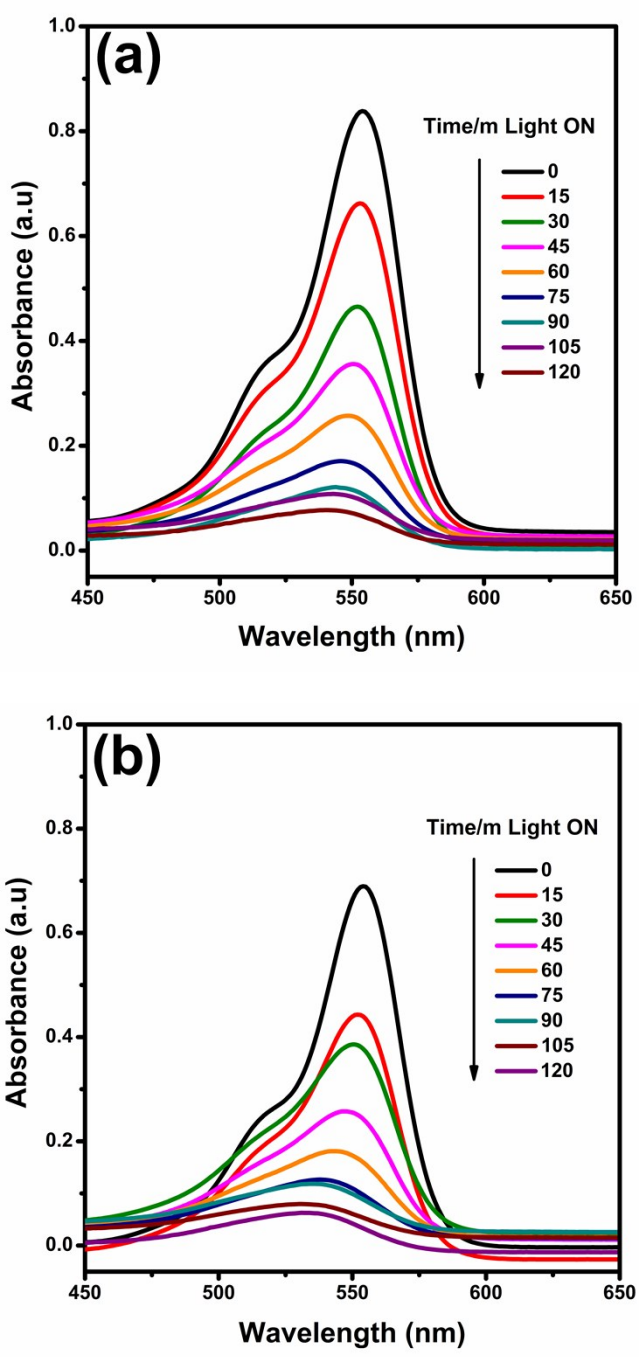

Fig. S12 Absorbance spectra depicting the change in concentration of Rhodamine B over nanocomposite under visible irradiation as a function of time namely, **(a)** Cu_2O/SnO_2 = 2:1 and **(b)** Cu_2O/SnO_2 = 1.5:1.

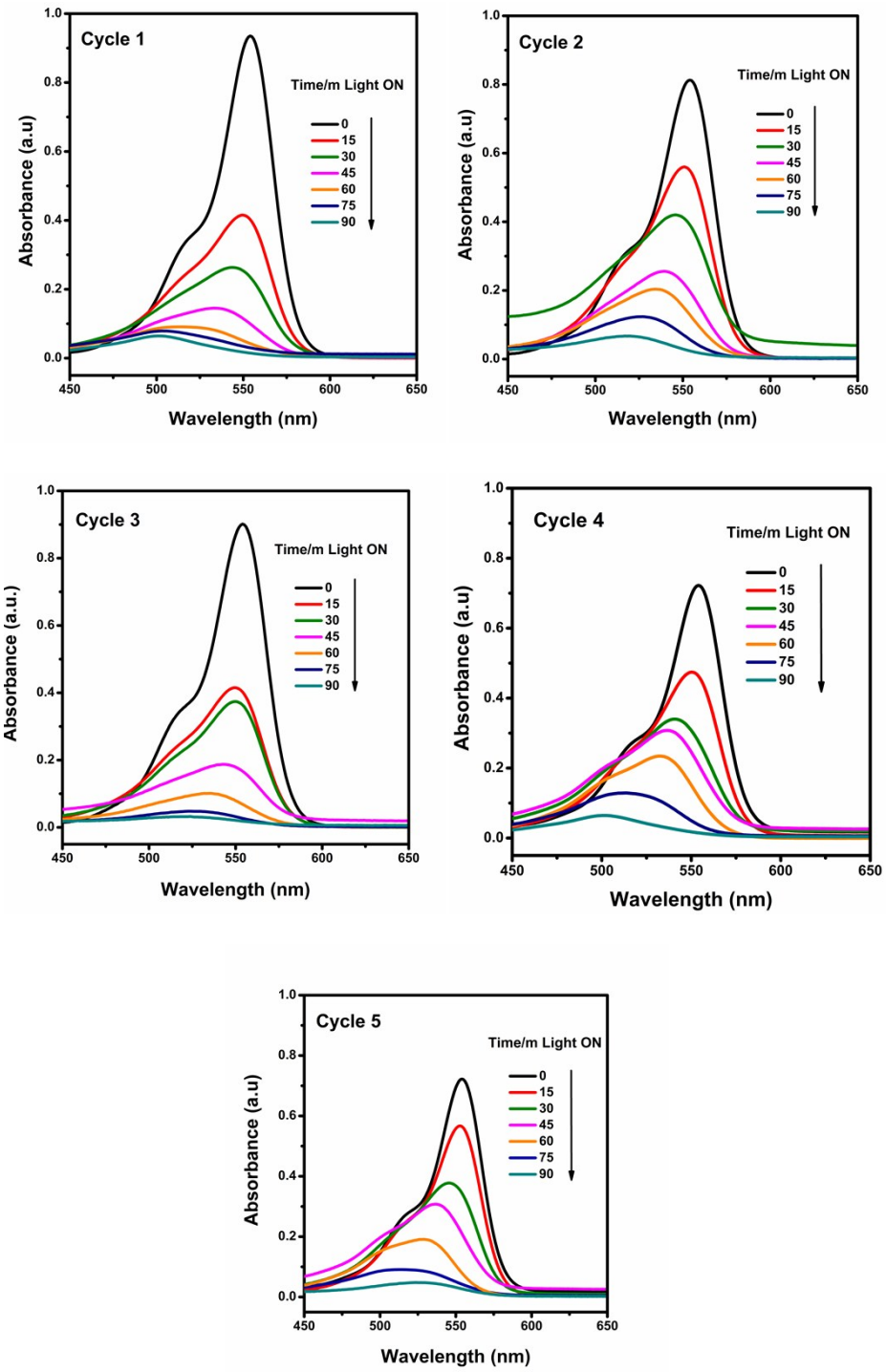

Fig. S13 Absorbance spectra depicting the change in concentration of Rhodamine B over Cu_2O/SnO_2 nanocomposite in 1:1 mole ratio for five successive cycles under visible irradiation as a function of time.

Spectrum processing :

Peak possibly omitted : 1.734 keV

Processing option : All elements analyzed (Normalised)

Number of iterations = 3

Standard :

C CaCO3 1-Jun-1999 12:00 AM

O SiO2 1-Jun-1999 12:00 AM

Cu Cu 1-Jun-1999 12:00 AM

Sn Sn 1-Jun-1999 12:00 AM

Element	Weight%	Atomic%
C K	6.70	17.34
O K	32.52	63.22
Cu L	15.45	7.56
Sn L	45.33	11.88
Totals	100.00	

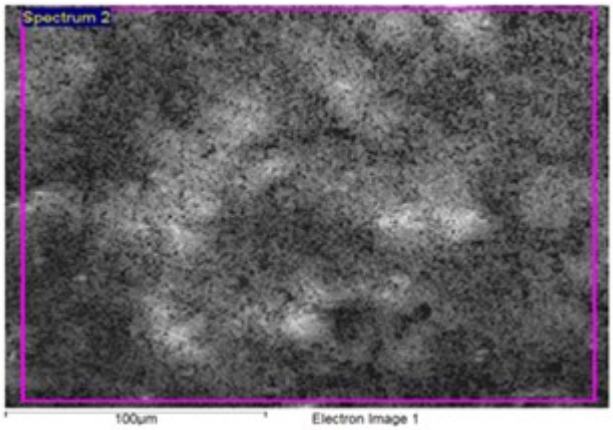

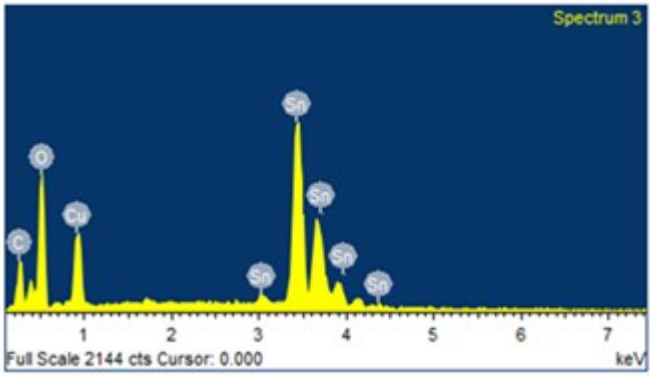

Fig. S14 Elemental analysis of Cu_2O/SnO_2 nanocomposite synthesized in 1:1 ratio after five consecutive cycles of visible light induced Rhodamine B photodegradation.

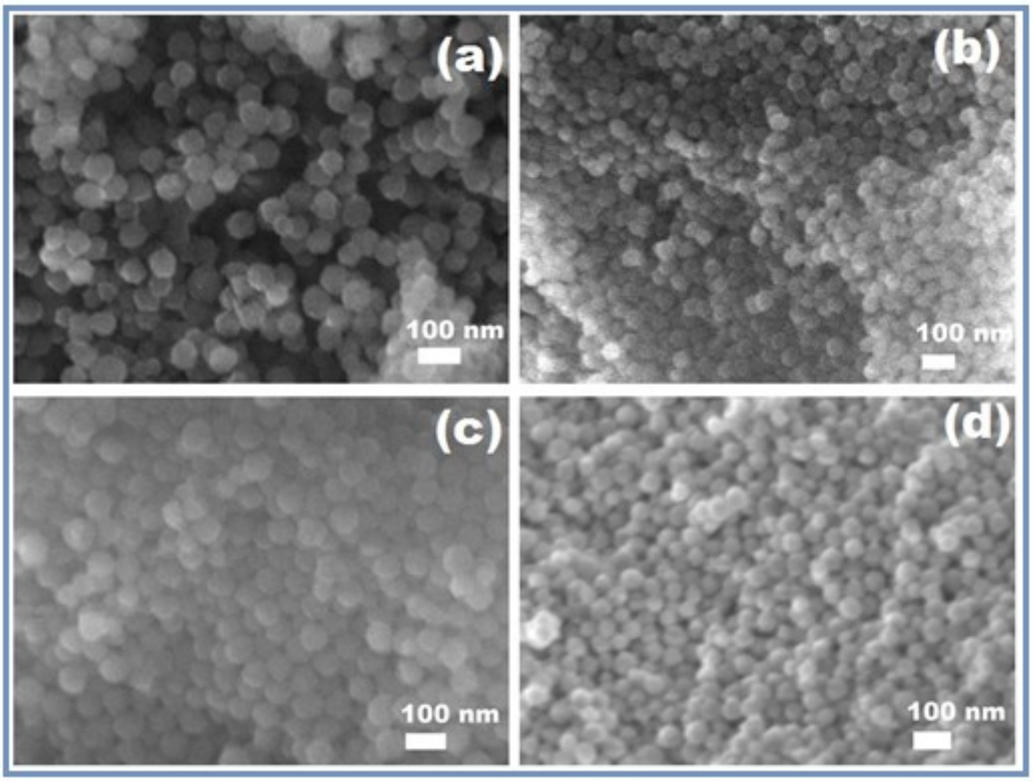

Fig. S15 (a-d) FE-SEM images of 1:1 mole ratio Cu_2O/SnO_2 nanocomposite after five successive cycles of visible light induced Rhodamine B photodegradation.

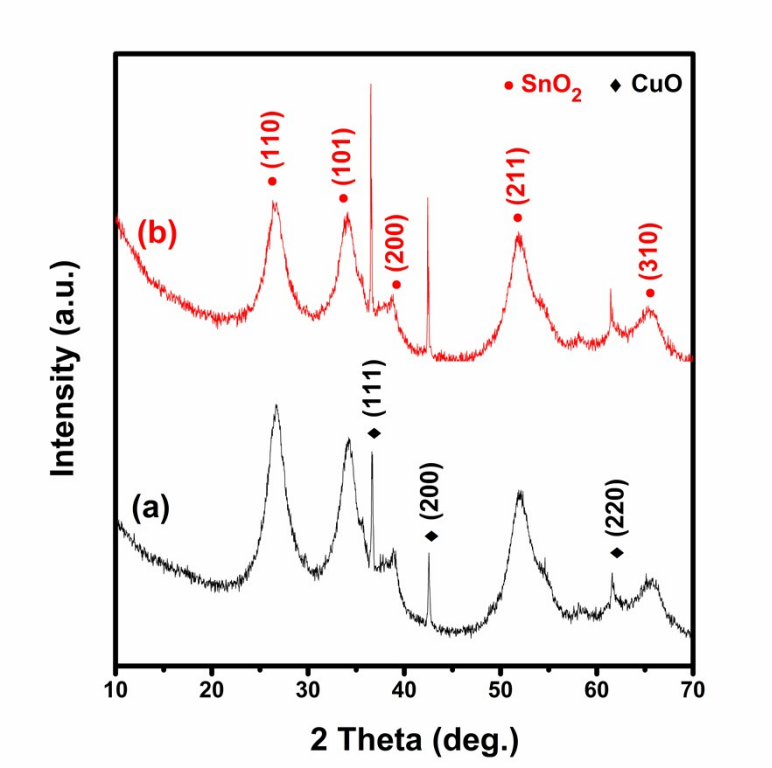

Fig. S16 X-ray diffraction patterns of Cu_2O impregnated in SnO_2 matrix to form nanocomposites in 1:1 mole ratio **(a)** before photodegradation and **(b)** after five successive cycles of visible light induced Rhodamine B photodegradation.

Supplementary References

1 Lin, Z.; Han, D.; Li, S. Study on Thermal Decomposition of Copper (II) Acetate Monohydrate in Air. *J. Therm Anal. Calorim.* 2012, **107**, 471-475.

2 Manjula, P.; Ramireddy, B.; Manorama, S.V. A Facile And Green Approach for the Controlled Synthesis of Porous SnO_2 Nanospheres: Application as an Efficient Photocatalyst and an Excellent Gas Sensing Material. *ACS Appl. Mater. Inter.* 2012, **4**, 6252-6260.

3 Nandapure, B.; Kondawar, S.; Salunkhe, M.; Nandapure, A. Nanostructure Cobalt Oxide Reinforced Conductive and Magnetic Polyaniline Nanocomposites. *J. Compos. Mater.* 2013, **47**, 559.

4 Jonynaite, D.; Senvaitiene, J.; Beganskiene, A.; Kareiva, A. Spectroscopic Analysis of Blue Cobalt Smalt Pigment. *Vib. Spectrosc.* 2010, **52**, 158-162.

5 Gu, F.; Wang, S. F.; Lu, M. K. Luminescent Properties of Mn^{2+} - Doped SnO_2 Nanoparticles. *Inorg. Chem. Commun.* 2003, **6**, 882-885.

6 Zaki, M. I.; Hasan, M. A.; Pasupulety, I. Influence of CuO_x Additives on CO Oxidation Activity and Related Surface and Bulk Behaviours of Mn_2O_3, Cr_2O_3 and WO_3 Catalysts. *Appl. Catal. A*. 2000, **198**, 247-259.

7 Grazenaite, E.; Kiuberis, J.; Beganskiene, A.; Senvaitiene, J.; Kareiva, A. XRD and FTIR Characterisation of Historical Green Pigments and their Lead-based Glazes. *Chemija.* 2014, **25**, 199-205.

8 Mageshwari, K.; Sathyamoorthy, R. Flower shaped CuO Nanostructures-Synthesis Characterization and Antimicrobial Activity. *J. Mater. Sci. Technol.* 2013, **29**, 909-914.

9 Xu, Y.Y.; Chen, D.R.; Jiao, M.L.; Xue, K.Y. CuO microflowers composed of nanosheets: Synthesis, characterization, and formation mechanism. *Mater. Res. Bull.* 2007, **42**, 1723-1731.

10 Wang, S.L.; Xu, H.; Qian, L.Q.; Jia, X.; Wang, J.W.; Liu, Y.Y.; Tang, W.H. CTAB-assisted Synthesis and Photocatalytic Property of CuO Hollow Microspheres. *J. Solid. State. Chem.* 2009, **182**, 1088-1093.

11 Kumar, V., Govind, A., Nagarajan, R. Optical and Photocatalytic Properties of Heavily F-Doped SnO_2 Nanocrystals by a Novel Single-Source Precursor Approach. *Inorg. Chem.* 2011, **50**, 5637–5645.

12 Park, M. S.; Wang, G. X.; Kang, Y. M.; Wexler, D.; Dou, S.X.; Liu, H. K. Preparation and Electrochemical Properties of SnO_2 Nanowires for Application in Lithium-Ion Batteries, *Angew. Chem., Int. Ed.* 2007, **46**, 750-767.

13 Cheng, G., Wang, J., Liu, X., and Huang, K. Self-Assembly Synthesis of Single-Crystalline Tin Oxide Nanostructures by A Poly (Acrylic Acid)-Assisted Solvothermal Process. *J. Phys. Chem. B,* 2006, **110**, 16208–16211.

14 Yu, K. N., Xiong, Y., Liu, Y., Xiong, C. Microstructural Change of Nano-SnO_2 Grain Assemblages with the Annealing Temperature. *Phys. Rev.B.* 1997, **55**, 2666-2671.

15 Shanmugasundaram, A.; Basak, P.; Satyanarayana, L.; Manorama, S.V. Hierarchical SnO/SnO_2 Nanocomposites: Formation of *in-Situ p-n* Junctions and Enhanced H_2 Sensing. *Sensor Actuat B: Chem.* 2013, **185**, 265-273.

16 Cheng, B.; Russe, J. M.; Shi, W.; Zhang, L.; Samulski, E. T. Large-Scale Solution-Phase Growth of Single-Crystalline SnO_2 Nanorods. *J. Am. Chem. Soc.* 2004, **126**, 5972-5973.

17 Zuo, J.; Xu, C.; Liu, X.; Wang, C.; Wang. C.; Hu, Y.; Qian, Y. Study of the Raman Spectrum of Nanometer SnO_2. *J. Appl. Phys.* 1994, **75**, 1835-1838.

18 Wang, N., Cao, X., Cai, X., Xu, Y., and Guo, L. Porous Cuprite Films: Facile Solution Deposition and their Application for Nitrite Sensing. *Analyst.* 2010, **135**, 2106-2110.

19 Chan, H. Y. H., Takoudis, C. G., and Weaver, M. J. Electrochemical Control of Gas-Phase Oxidation and Reduction of Copper as Probed by Surface-Enhanced Raman Spectroscopy. *Electrochem. Solid State Lett.* 1999, **2**, 189-191.

20 Chan, H. Y. H., Takoudis, C. G., and Weaver, M. J. Oxide film formation and Oxygen Adsorption on Copper in Aqueous Media as Probed by Surface-Enhanced Raman Spectroscopy. *J. Phys. Chem. B.* 1999, **103**, 357-366.

21 Lefevre, G., Walcarius, A., Ehrhardt, J. J., and Bessiere, J. Sorption of Iodide on Cuprite (Cu_2O). *Langmuir*, 2000, **16**, 4519-4527.

22 Chrzanowske, J., and Irwin, J. C. Raman Scattering from Cupric Oxide. *Solid State Commun*. 1989, **70**, 11-14.

23 Goldstein, H. F., Kim, D. S., Yu, P. Y., and Bourne, L. C. Raman Study of CuO Single Crystals. *Phys. Rev. B.* 1990, **41**, 7192-7198.

24 Xu, J. F., Ji, W., Shen, Z. X., Li, W. S., Tang, S. H., Ye, X. R., Jia, D. Z., and Xin, X. Q. Raman Spectra of CuO Nanocrystals. J. *Raman Spectrosc.* 1999, **30**, 413-415.

25 Zhang, Y. P., Pan, C. X. TiO_2/graphene Composite from Thermal Reaction of Graphene Oxide and its Photocatalytic Activity in Visible Light. *J. Mater. Sci.* 2011, **46**, 2622-2626.

26 Zhang, D. Synergetic Effects of Cu_2O Photocatalyst with Titania and Enhanced Photoactivity under Visible Irradiation. *Acta Chimica Slovaca.* 2013, **6**, 141-149.

27 Hu, J. Q., Ma, X. L., Shang, N. G., Xie, Z. Y., Wong, N. B., Lee, C. S., and Lee. S. T. Large-Scale Rapid Oxidation Synthesis of SnO_2 Nanoribbons. J. Phys. Chem. B. 2002, **106**, 3823-3826.

28 Hu, J., Bando, Y., Liu, Q., Golberg, D. Laser Abalation Growth and Optical Properties of Wide And Long Single Crystal SnO_2 Ribbons. *Adv. Funct. Mater.* 2003, **13**, 493-496.

29 Panigrahy, B., Aslam, M., Misra, D. S., Ghosh, M., Bahadur, D. Defect-related Emissions and Magnetization Properties of ZnO Nanorods. *Adv. Funct. Mater.* 2010, **20**, 1161-1165.

30 Ghosh, M., Ningthoujam, R., Vatsa, R., Das, D., Nataraju, V., Gadkari, S., Gupta, S., Bahadur, D. Role of Ambient Air on Photoluminescence and Electrical Conductivity of Assembly of ZnO Nanoparticles. *J. Appl. Phys.* 2011, 110, 054307-054309.

31 Kar, A., Stroscio, M.A., Dutta, M., Kumari, J., Meyyappan, M. Observation of Ultraviolet Emission and Effect of Surface States on the Luminescence from Tin Oxide Nanowires, *Appl. Phys. Lett.* 2009, **94**, 101905-101908.

32 Khoang, N.D., Trung, D.D., Van Duy, N., Hoa, N.D., Van Hieu, N. Design of SnO_2/ZnO Hierarchical Nanostructures for Enhanced Ethanol Gas-Sensing Performance, *Sensor Actuat B: Chem.* 2012, **174**, 594-601.

33 Prevot, B., Carabatos, C., and Sieskind, M. Infrared Absorption in Cu_2O after Annealing in Oxygen or He+ Particles Bombardments. *Phys. Status. Solidi. A.* 1972, **10**, 455-463.